

A pressure-sensitive rheological origin of high friction angles of granular matter observed in NASA-MGM project

Xiaohui Cheng(程晓辉), Shize Xiao(肖世泽), Sen Yang(杨森), Naifeng Zhao(赵乃峰), and Alex Sixie Cao

Citation: Chin. Phys. B, 2024, 33 (**6**): 068301. DOI: 10.1088/1674-1056/ad3b88
Journal homepage: http://cpb.iphy.ac.cn; http://iopscience.iop.org/cpb

What follows is a list of articles you may be interested in

Correlation mechanism between force chains and friction mechanism during powder compaction

Ning Zhang(张宁), Shuai Zhang(张帅), Jian-Jun Tan(谈健君), and Wei Zhang(张炜)
Chin. Phys. B, 2022, 31 (**2**): 024501. DOI: 10.1088/1674-1056/ac0db1

High coercivity in large exchange-bias Co/CoO-MgO nano-granular films

Ge Chuan-Nan (葛传楠), Wan Xian-Gang (万贤纲), Eric Pellegrin, Hu Zhi-Wei (胡志伟), Wen-I Liang, Michael Bruns, Zou Wen-Qin (邹文琴), Du You-Wei (都有为)
Chin. Phys. B, 2015, 24 (**3**): 034501. DOI: 10.1088/1674-1056/24/3/034501

Fast synchrotron X-ray tomography study of the packing structures of rods with different aspect ratios

Zhang Xiao-Dan (张晓丹), Xia Cheng-Jie (夏成杰), Xiao Xiang-Hui (肖相辉), Wang Yu-Jie (王宇杰)
Chin. Phys. B, 2014, 23 (**4**): 044501. DOI: 10.1088/1674-1056/23/4/044501

Dependence of effective screening length in granular columns on bead and silo sizes and their ratio

Ali Shah, Ahmed Khan, Saeed Ahmed Khan
Chin. Phys. B, 2013, 22 (**5**): 058301. DOI: 10.1088/1674-1056/22/5/058301

A pressure-sensitive rheological origin of high friction angles of granular matter observed in NASA–MGM project

Xiaohui Cheng(程晓辉)[1,†], Shize Xiao(肖世泽)[1], Sen Yang(杨森)[1], Naifeng Zhao(赵乃峰)[2,‡], and Alex Sixie Cao[1,3]

[1] *Department of Civil Engineering, Tsinghua University, Bejing* 100084, *China*
[2] *College of Transportation Engineering, Nanjing Tech University, Nanjing* 211816, *China*
[3] *Institute of Structural Engineering, ETH Zurich, Zurich* 8092, *Switzerland*

(Received 6 March 2024; revised manuscript received 21 March 2024; accepted manuscript online 7 April 2024)

An abnormally high peak friction angle of Ottawa sand was observed in (National Aeronautics and Space Administration) NASA–(Mechanics of Granular Materials) MGM tests in microgravity conditions on the space shuttle. Previous investigations have been unsuccessful in providing a constitutive insight into this behavior of granular materials under extremely low effective stress conditions. Here, a recently proposed unified constitutive model for transient rheological behavior of sand and other granular materials is adopted for the analytical assessment of high peak friction angles. For the first time, this long-eluded behavior of sand is attributed to a hidden rheological transition mechanism, that is not only rate-sensitive, but also pressure-sensitive. The NASA–MGM microgravity conditions show that shear-tests of sand can be performed under abnormally low confining stress conditions. The pressure-sensitive behavior of granular shearing that is previously ignored is studied based on the $\mu(I)$ rheology and its variations. Comparisons between the model and the NASA microgravity tests demonstrate a high degree of agreement. The research is highly valid for pressure-sensitive and rate-dependent problems that occur during earthquakes, landslides, and space exploration.

Keywords: granular matter, microgravity, pressure-sensitive, NASA–MGM

PACS: 83.80.Fg, 45.70.Cc **DOI:** 10.1088/1674-1056/ad3b88

1. Introduction

Outer space granular matter is subjected to very low effective stress in low and microgravity environments, and the granular matter exhibits completely different physical and mechanical properties than under 1-g conditions. The study of low and microgravity granular matter rheology has become an important topic in microgravity science research, and this research is of great value not only for space exploration engineering, but also for earth seismic liquefaction engineering and granular matter phase transition research. The background of this paper is the preliminary theoretical preparation for the "Variable Gravity Granular Shear Rheology Experiment", an ongoing project on the Chinese manned space station. In the 1990s, the National Aeronautics and Space Administration–Mechanics of Granular Materials (NASA–MGM) project[1] conducted a quasi-static triaxial shear experiment on dry sand on board the space shuttle, and the high peak friction angle characteristics of the sand were very puzzling. The axial strain rate used in the experiments is still in the range of quasi-static loading rates of conventional ground experiments, but the effective stress can be reduced to the level of one percent of the earth's surface. According to the recently developed theory of granular rheology, i.e., $\mu(I)$ rheology, the reduction of the effective stress also excites the shear rheological properties of the granular material, just like the increase of the external loading rate, leading to the increase of the intrinsic viscous stress. In this context, the goal of this paper is to demonstrate the rheological causes of the high peak friction angle phenomenon in the microgravity triaxial shear experiment of dry sand in the NASA–MGM project, and to provide a scientific basis and new perspective for the design and optimization of granular shear rheology experiments on the Chinese manned space station.

In soil mechanics and geotechnical engineering, the rate-dependent behavior of sand for common levels of effective stress of more than ~ 10 kPa has been the focus of research for a long time. Such behavior of sand and other granular materials becomes significant for shear strain rates of more than $\sim 10^{-3}$ s^{-1}. Such strain rates occur during seismic liquefaction events and landslides. For shear strain rates of less than $\sim 10^{-3}$ s^{-1}, the behavior of sand can be considered as quasi-static and therefore, rate-independent. In this regime, the frictional resistance of sand can be studied and modelled using the critical state soil mechanics, elastoplastic solid mechanics, and granular discrete element methods. However, triaxial shear tests performed in the NASA–MGM project on Ottawa sand in microgravity environments showed abnormally high peak friction angles.[1] This was only observed under microgravity conditions. Shear strain rates used in the NASA–

†Corresponding author. E-mail: chengxh@tsinghua.edu.cn
‡Corresponding author. E-mail: zhaonaifeng@njtech.edu.cn

© 2024 Chinese Physical Society and IOP Publishing Ltd

MGM microgravity tests stay the same as in quasi-static triaxial shear tests conducted in any soil mechanics laboratories worldwide. But due to the microgravity environment of NASA–MGM project, the effective isotropic stress or the confining stress of the specimen was reduced to extremely low levels of less than ~ 10 kPa.

Various explanations have been proposed for the abnormally high peak friction angles in the NASA microgravity tests. These include experimental errors,[2] cohesive forces,[1] sand particle interlocking,[3] tungsten carbide panel friction,[4] and extra confining pressure from the latex membranes in the experiments.[2] Jeremic *et al.*[2] developed a rate-independent hyperelastic model coupled with a plastic hardening and softening model by introducing an equivalent relative density and friction hardening parameters. This model is generally able to describe shear-dilated hardening before the peak friction angle and post-peak softening of Ottawa sand.

In the NASA microgravity tests, the peak stresses occurred for axial strain levels of less than 0.5%. In addition, the peak axial strain decreased as the confining stresses became smaller. These observations deviate significantly from the model developed by Jeremic *et al.*[2] The sands that were tested were either medium dense or dense. For such sands, the occurrence of stress peaks is a relatively regular phenomenon in a normal gravity environment. However, the occurrence of very high stress peaks at strains of less than 0.5% should not be directly related to the elastoplastic hardening and softening characteristics of a solid material. Since the model developed by Jeremic *et al.*[2] is a rate-independent elastoplastic solid mechanics model, it is unable to correctly reflect the rheological mechanisms that may occur in granular materials at very low effective stress levels.

Sand and other granular materials show solid and fluid-like transitional behavior that are dramatically affected by the effective stress level and the shear rate. Studies on the rheology for granular materials over the last two decades (e.g., MiDi, 2004,[5] Forterre and Pouliquen, 2008,[6] Jiang and Liu, 2015,[7] Li *et al.*, 2023[8]) have shown that a pressure-sensitive granular viscosity is present. Unlike common non-Newtonian fluids, this granular viscosity has exhibited significant dependency on the effective stress level. This behavior has also been observed even for quasi-static strain rates under very low effective stress levels.[9] A unified constitutive model has been proposed and validated against novel triaxial shear flow tests. The proposed model uses two dimensionless physical parameters to improve the description of total shear stress that includes both quasi-static and viscous components in granular materials. At extremely low effective stress levels, "granular viscosity" becomes the primary mechanism that suppresses the quasi-static behavior, even for common quasi-static shear strain rates. The pressure-sensitive and rate-dependent viscous stress in granular materials can become significant in microgravity environments which are severely different from 1-*g* environments on the Earth.

In this paper, an investigation of experimental error analysis is first carried out to show that different experimental errors that have been questioned in the past are not the main reason for the abnormally high peak friction angles in the NASA microgravity tests. Subsequently, the mathematical formulation of our previously developed unified constitutive model is presented. Based on this model, a new pressure sensitive rheological mechanism of granular matter is first proposed for the peak friction angle issue for a triaxial test environment under microgravity conditions. Furthermore, an MATLAB subroutine is developed to simulate in details the shear stresses and the friction angles in the NASA microgravity tests for the axial and radial strain rates present in a triaxial environment. To our knowledge, this is the first explanation of a newly discovered physical mechanism which elucidates the high peak friction angles observed in the NASA microgravity tests. This new physical mechanism plays a vital role in microgravity granular matter study in Chinese manned space station and other microgravity platforms.

2. Investigation of high peak friction angles

In the NASA microgravity tests, nine sets of conventional triaxial shear tests were conducted in a microgravity environment on space shuttles. The triaxial shear test applies pressure to the cylindrical specimen in the three coordinate directions of space. The test is performed by first subjecting the specimen to the same confining pressure in all three axes (the magnitude of which is determined by a manometer) through a pressurized fluid in the pressure chamber and maintaining it constant throughout the test in case of conventional triaxial shear scheme. Then the vertical axial stress is applied to the specimen through the piston until the specimen is sheared to the failure. The tests were carried out by NASA scientists on dry Ottawa sand with 65% and 85% relative densities, an axial strain rate of 6.5×10^{-5} s^{-1}, and confining pressures of 0.05 kPa, 0.52 kPa, and 1.30 kPa, respectively. A description detailing the test regime is given in Sture *et al.*[1] A photograph of a typical cylindrical sample is included in Section S2 of supporting information.

The triaxial shear experimental data in this paper are quoted from the published literature of the NASA–MGM project if not otherwise specified. To ensure repeatable test data, five small load loading and unloading cycles were performed at a specific shear stress–strain point. Figure 1 shows an example of the principal stress ratio σ_a/σ_r versus axial strain ε_a for one set of the tests. The other tests have the same characteristics as the one shown here. In Fig. 1, the peak stress ratio occurs at an axial strain of about 0.005, after which the

specimen enters a softening regime. Subsequently, the sample enters a critical or residual state where the principal stress ratio appears to be stabilized. The apparent friction angle and peak and critical stress ratios from the microgravity and 1-g environments are collated in Section S1 of supporting information. The apparent friction angle φ was computed from the following equation:

$$\sin\varphi = \frac{\sigma_a - \sigma_r}{\sigma_a + \sigma_r}, \tag{1}$$

where σ_a is the axial principal stress and σ_r is the confining pressure or radial principal stress. This is the same expression that was used originally by NASA.[1] In Eq. (1), it is assumed that the granular material with no cohesion follows the Mohr–Coulomb strength criterion, which is literally the friction law of deformable materials in terms of normal and shear stresses.[10] In contrast, conventional friction law of rigid materials is defined in terms of normal and frictional forces. The peak and critical friction angles of Ottawa sand are calculated by submitting the peak and critical state axial and confining pressure listed in Table S1 of supporting information into Eq. (1), respectively. Thus, the peak and critical state friction angles correspond to the peak stress state and the so-called critical stress state where the stress is stable and constant at large strains after softening, respectively. Two stress states are shown in Fig. 1, respectively.

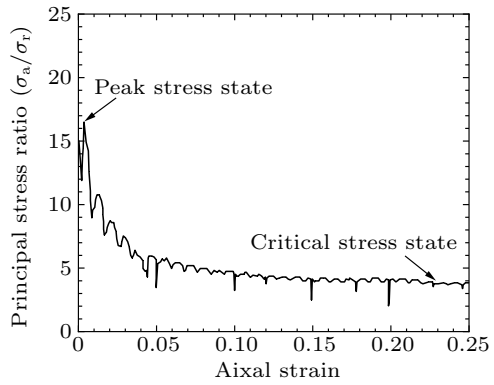


Fig. 1. Principal stress ratio σ_a/σ_r versus axial strain rate ε_a curve of the test with a relative density of $D_r = 85\%$ and a confining pressure of 0.05 kPa. Modified from Sture *et al.*[1]

Figure 2 shows the relationship between the calculated peak friction angle φ_p in red and the critical friction angle φ_s in blue, and the confining pressure σ_r. The results show that dry sand has a significantly higher peak friction angle φ_p for low confining pressures σ_r than for high confining pressures σ_r. The critical friction angle φ_s does not change much for the different confining pressures.

Tests in geotechnical engineering and granular physics are usually carried out in a 1-g environment. The NASA microgravity tests were conducted in a microgravity environment with extremely low to low confining pressures. It is generally accepted that the main sources of error affecting the results of triaxial experiments are the ending friction, the membrane stress of the latex membrane and the cohesion of the granular sample itself. Since the tests were carried out in unusual conditions, an investigation into possible sources for errors or deviations were carried out in Section S2 of supporting information. Here, the effects of dry sand cohesion, granular interlocking, friction from the tungsten-carbide loading panels, and extra confining pressure on the high peak friction angle from the latex membrane are investigated with a detailed discussion. None of the investigated sources for errors or deviations were sufficient to cause the high peak friction angles observed in the tests.

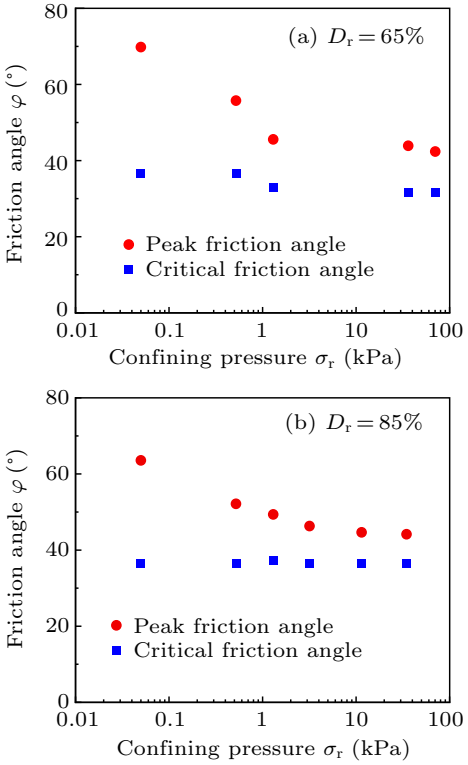


Fig. 2. Peak friction angle φ_p (red) and critical friction angle φ_s (blue) versus effective confining pressure for a relative density of 65% and 85%.

3. Extended $\mu(I)$ rheology

Based on the results of the microgravity tests, NASA researchers developed a complex hyperelastic plastic constitutive model with hardening and softening plasticity.[2] Their model was implemented in large-deformation finite element calculations with the aim of explaining the abnormally high peak friction angles and the complete stress–strain curves at very low confining pressures observed in the experiments. This behavior is illustrated in Figs. 1 and 2. However, traditional elastoplastic solid mechanics is not valid for the conditions of the NASA microgravity tests. At very low effective stresses, granular solid materials can exhibit a phase transition between a solid-like state to a fluid-like state. In the phase transition from solid-like to liquid-like, solid elastoplastic behav-

ior is reduced and rate-dependent viscous behavior becomes ever more present. At some point, the rate-dependent viscous effects become sufficiently significant such that the behavior of the granular material can no longer solely be described from the perspective of elastoplastic solid mechanics.

The inertial number I in the original formulation of $\mu(I)$ rheology is given by[5,11]

$$I = \dot{\gamma} d \sqrt{\frac{\rho_s}{p}} = \frac{T_p}{T_m}, \tag{2}$$

where the inertia number I reflects the influence of the shear strain rate $\dot{\gamma}$ and the effective stress level p on the viscous behaviour of granular materials. It can be expressed as the ratio between the microscopic time scale T_p and the macroscopic timescale T_m of the particles. The microscopic time scale T_p is the time required for a particle with diameter d for an effective stress p to undergo a particle misalignment when an interlayer misalignment occurs. It represents the rapidity of microscopic particle rearrangement that is pressure sensitive. T_m represents the macroscopic shear strain rate and ρ_s is the density.

An S-shaped relation between the pressure-sensitive viscous shear stress and shear strain-rate in granular materials is observed. An illustration showing the relation between the viscous shear stress ratio q_v/q_s ($q_v = \mu_v p$, $q_s = \mu_s p$, μ_v and μ_s are presented in Fig. 4) and the shear strain rate $\dot{\gamma}$ based on the original $\mu(I)$ rheology is shown in Fig. 3. In conventional soil mechanics tests, the shear strain rates $\dot{\gamma}$ are typically less than 10^{-5} s^{-1} and typical effective stresses are in the order of multiples of 10 kPa. In such tests, the viscous stress and rate-dependent response can generally be neglected. However, the rate-dependent and viscous shear stress cannot be ignored for very low effective stresses such as in the NASA microgravity tests, even under common quasi-static strain rates.

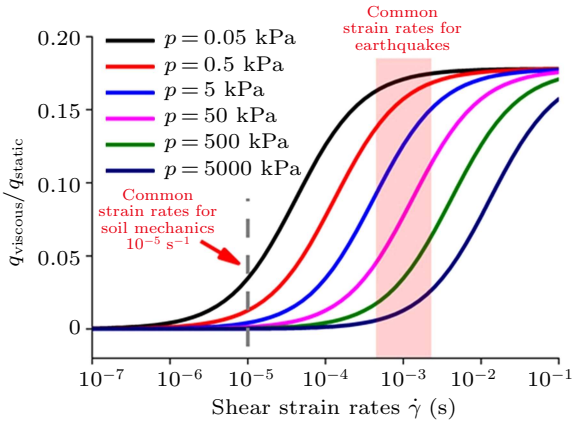


Fig. 3. Illustration of the relationship between the viscous stress ratio q_v/q_s and the shear strain rate $\dot{\gamma}$ based on the proposed model.[12]

Other researchers have explained the sources of different types of rate-dependent behavior in granular materials.[13–15] Sources include the irregularity of particle shapes, particle grades, particle size, crushing of particles, particle interlocking, and more. However, these sources have been provided based on the microstructural properties of the granular material. From our previous work, rate-dependent behavior of sand cannot be solely attributed to the microstructural properties alone and the interaction between the particles should also be considered. This interaction is not only dependent on the microstructural properties themselves, but also on external factors such as the effective stress p and the shear strain rate $\dot{\gamma}$. For very low effective stresses p, sand may respond in a rate-dependent, pressure-sensitive, and viscous manner. This holds even for very low shear strain rates $\dot{\gamma}$. The described behavior is attributed to the low natural frequency and increased viscosity in such conditions. This behavior is believed to be responsible for the large peak friction angles φ_p observed by Sture *et al.* in the NASA microgravity tests.

In the original formulation of $\mu(I)$ rheology, the viscous shear stress cannot be accurately calculated for non-steady granular shear flows. To extend this steady-state rheological model to transient granular flows, we developed a unified constitutive model. Figure 4 shows the conceptual framework of the new model, where the relation between the effective friction coefficient μ and the shear strain γ is shown. The effective friction coefficient μ is defined as

$$\mu = \frac{\tau}{p}, \tag{3}$$

where τ is the total shear stress, and p is the effective isotropic stress.

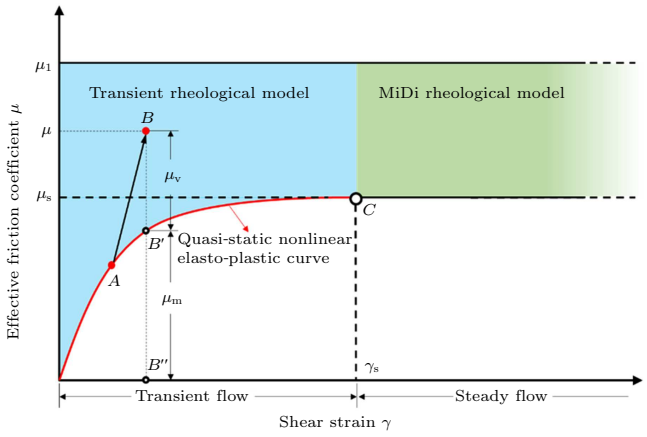


Fig. 4. Conceptual framework of the unified constitutive model.

In Fig. 4, the curved red line $\widehat{OC}$ is the quasi-static solid-like stress–strain relation described by traditional geotechnics. The blue area above the curved red line $\widehat{OC}$ is the domain of transient flow which can be better described by our new unified model. The green area above the flat line is the domain of steady transient flow which can be described by the original $\mu(I)$ rheology. The upper flat line μ_1 signifies the threshold between a steady dense flow for $\mu < \mu_1$, and an accelerated unsteady dense flow for $\mu > \mu_1$. In our unified model, the threshold μ_1 remains unchanged. The distance from the shear

strain axis γ to the curved red line $\widehat{OC}$ is the mobilized friction coefficient $\mu_{\rm m}$, which is a new parameter in our unified model. The mobilized friction coefficient $\mu_{\rm m}$ represents the stress–strain relation in a quasi-static state and its upper bound $\mu_{\rm s}$ is the critical friction coefficient. The critical friction coefficient $\mu_{\rm s}$ signifies the threshold between a quasi-static state for $\mu < \mu_{\rm m}$ and a moderate shear flow for $\mu > \mu_{\rm m}$.

For the NASA microgravity tests, the original $\mu(I)$ rheology is inaccurate as it does not separate the mobilized friction coefficient $\mu_{\rm m}$ and the critical friction coefficient $\mu_{\rm s}$. Due to this, the original $\mu(I)$ rheology neglects the moderate flow state bounded by the quasi-static elastoplastic curve $\widehat{OC}$ and the critical friction coefficient $\mu_{\rm s}$ in Fig. 4. Another limitation of the original $\mu(I)$ rheology is its inability to separate the stress components between the viscous part $\tau_{\rm v}$ and the quasi-static part $\tau_{\rm s}$. Our unified model is summarized in Section S3 of supporting information. For the following analysis purpose in this paper, the axisymmetric version is presented in the next section.

4. Analytical solution for high peak friction angles

In the NASA microgravity tests, conventional triaxial tests were conducted in a microgravity environment. Thus, the constitutive equations that are established in this section are also for a triaxial environment. These are based on the unified model summarized in Section S3 of supporting information. The total stress σ_{ij} tensor is defined as

$$\sigma_{ij} = p\delta_{ij} + u_{\rm m}p + \mu_{\rm v}(I)\, p\frac{2\dot{e}_{ij}}{\dot{\gamma}}, \tag{4}$$

where p is the effective isotropic stress, δ_{ij} is the Kronecker delta, $\mu(I)$ is the dynamic friction coefficient as a function of the inertial number I, $\dot{e}$ is the deviatoric strain rate tensor, and $\dot{\gamma}$ is the magnitude or the second invariant of the engineering shear strain rate tensor $\dot{\gamma}_{ij}$. Following Eq. (4), the axial $\sigma_{\rm a}$ and radial $\sigma_{\rm r}$ principal stresses in a triaxial environment can be expressed as

$$\frac{\sigma_{\rm a,r}}{p} = 1 + \frac{2Ge_{\rm a,r}}{p} + \mu_{\rm v}\frac{2\dot{e}_{\rm a,r}}{\dot{\gamma}}, \tag{5a}$$

$$\mu_{\rm v} = \frac{\mu_1 - \mu_{\rm m}}{\dfrac{I_0}{I} + 1}, \tag{5b}$$

$$\mu_{\rm m} = \frac{G\gamma}{p}, \tag{5c}$$

$$G(\gamma) = \frac{A(\gamma)\, p_{\rm a}}{(1+e)^3}\left(\frac{p}{p_{\rm a}}\right)^{m(\gamma)}, \tag{5d}$$

$$A(\gamma) = \frac{A_0}{1+\gamma/\gamma_{\rm r2}}, \tag{5e}$$

$$m(\gamma) = 0.5 + \frac{0.5}{1+\gamma_{\rm r1}/\gamma}, \tag{5f}$$

where the subscript "a" indicates the axial direction, "r" indicates the radial direction, and p is the effective isotropic stress, G is the secant quasi-static shear modulus as a function of the shear strain γ, $p_{\rm a} = 101.325$ kPa is the standard atmospheric pressure, e is the deviatoric strain, $\mu_{\rm v}$ is the viscous friction coefficient, $\mu_{\rm m}$ is the mobilized quasi-static friction coefficient, $\dot{e}$ is the deviatoric strain rate.

The deviatoric strains $e_{\rm a,r}$ and the magnitude of engineering shear strain γ are defined as

$$e_{\rm a} = \frac{2}{3}(\varepsilon_{\rm a} - \varepsilon_{\rm r}),\quad e_{\rm r} = -\frac{1}{3}(\varepsilon_{\rm a} - \varepsilon_{\rm r}),\quad \gamma = \frac{2}{\sqrt{3}}(\varepsilon_{\rm a} - \varepsilon_{\rm r}), \tag{6}$$

where $\varepsilon_{\rm a,r}$ are the axial and radial principal strains. In the triaxial environment, the principal stress ratio $\sigma_{\rm a}/\sigma_{\rm r}$ is calculated according to Eqs. (5a)–(5c)

$$\frac{\sigma_{\rm a}}{\sigma_{\rm r}} \equiv \frac{\sqrt{3} + 2(\mu_{\rm m} + u_{\rm v})}{\sqrt{3} - (\mu_{\rm m} + \mu_{\rm v})}. \tag{7}$$

To find the macroscopic friction angle φ, equation (7) can be substituted into Eq. (1)

$$\varphi = \arcsin\left[\frac{3}{1 + \dfrac{2\sqrt{3}}{\mu_{\rm m} + \mu_{\rm v}}}\right]. \tag{8}$$

Equation (8) provides an analytical expression for the macroscopic friction angle φ in a triaxial environment. The friction angle φ is dependent on both the quasi-static mobilized friction coefficient $\mu_{\rm m}$ and the viscous friction coefficient $\mu_{\rm v}$.

In a quasi-static 1-g environment, the viscous friction coefficient $\mu_{\rm v}$ in Eq. (5b) is small due to the small shear strain rate $\dot{\gamma}$ and the large effective stress p. In rate-independent critical state geotechnics, the viscous friction coefficient $\mu_{\rm v}$ is neglected and only the mobilized friction coefficient $\mu_{\rm m}$ is considered. This is also true for elastoplastic solid mechanics with hardening and softening. To compute the mobilized friction coefficient $\mu_{\rm m}$ in Eq. (5c), an empirical relation between the secant shear modulus G and the shear strain γ is used, see Section S3 of supporting information.

In a microgravity environment with quasi-static strain rates from a 1-g environment, the viscous friction coefficient increases even though the shear strain rate $\dot{\gamma}$ is in a quasi-static range for common effective stresses. The effective stresses in question are two to three magnitudes smaller than for a 1-g environment. Thus, the viscous friction coefficient $\mu_{\rm v}$ should not be negligible compared to the mobilized friction coefficient $\mu_{\rm m}$. This will result in a higher friction angle φ.

Table 1. Overview of model parameters.

Item	Parameter	Symbol (unit)	$D_r = 65\%$	$D_r = 85\%$
Basic physical parameter	maximum/minimum void ratio	e_{max}/e_{min}	0.790/0.502	
	dry density	ρ_s (kg/m^3)	2650	
	average grain diameter	d (mm)	0.22	
	void ratio	e	0.603	0.545
	apparent density	ρ (kg/m^3)	1653	1715
Quasi-static stress model parameters	critical state friction angle	φ_s (°)	37.0	37.0
	shear stiffness parameters	A_0	250	300
		γ_{r1} (%)	0.050	0.050
		γ_{r2} (%)	1.654	1.234
	bulk stiffness modulus	K (MPa)	50	50
Viscous shear stress model parameters	maximum viscous friction angle	φ_1 (°)	66.2	62.8
	reference inertial number	I_0	4.4×10^{-8}	5.0×10^{-8}

Note: $D_r = (e_{max} - e)/(e_{max} - e_{min})$.

5. Calculations of peak and critical friction angles

In this section, the peak φ_p and critical φ_s friction angles of the NASA microgravity tests were simulated. The simulations are based on the equations in Section 4 of the unified model derived for a triaxial test environment. All model parameters used for the simulation are listed in Table 1. All basic physical parameters are directly taken from the NASA–MGM experiments, and the critical sate friction angle is determined as the residual friction angel measured in the same experiments as well.[1] The parameter of A_0 is determined by measuring the initial shear modulus G_0 in Eqs. (5d)–(5f) for $\gamma = 0$, and the parameters of γ_{r1} and γ_{r2} are fit to the measured quasi-static triaxial stress–strain relationship of Ottawa sand. The maximum viscous friction angle of φ_1 is generally measured by sloping channel flow experiments and the reference initial number of I_0 is mainly related to the type of granular material, which can be also determined by sloping channel flow experiments. Detailed physical interpretation and calibration of model parameters are mentioned in Section S3 of supporting information. In order to calculate the peak and critical state friction angles, we need to use Eq. (8). There are two key variables involved in this equation. The mobilized friction coefficient μ_m is calculated by Eq. (5c), where the shear strain-dependent shear stiffness modulus G is obtained by Eqs. (5d)–(5f). And the viscous friction coefficient μ_v can be calculated by Eq. (5b), where the shear strain rate and pressure-dependent initial number I is calculated by Eq. (2). Therefore, μ_m is a function of the effective isotropic stress p and the shear strain γ, and μ_v is a function of the effective isotropic stress p, the shear strain γ and the shear strain rate $\dot{\gamma}$. The effective isotropic stress p can be calculated from the experimental data of stress ratio σ_a/σ_r and confining stress σ_r according to $p = \frac{1}{3}(\sigma_a + 2\sigma_r)$. The calculation procedure of γ and $\dot{\gamma}$ has been mentioned in Fig. 5, in which the calculated strain rates are shown in detail for the confining pressure 0.05 kPa as an example. Figure 5 shows the simulation results for the test specimens with relative densities of 65% and 85% subjected to a radial stress σ_r of 0.05 kPa. The simulation results are shown for the total friction coefficient μ, as well as the mobilized friction coefficient μ_m and the viscous friction coefficient μ_v. In addition, the results from the NASA microgravity tests are also shown in the same figures.

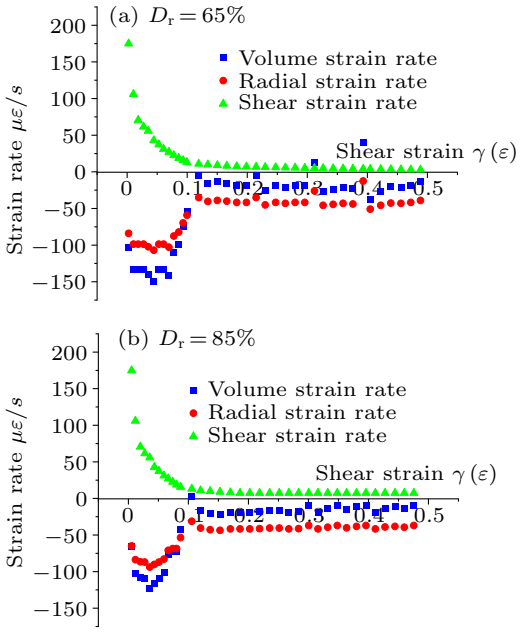


Fig. 5. Experimental results from the NASA microgravity tests on Ottawa sand ($\sigma_r = 0.05$ kPa). The constant axial strain rate $\dot{\varepsilon} = 64.8\mu\varepsilon/s$ and the volume strain rate $\dot{\varepsilon}$ is calculated from the $\varepsilon_a \sim \varepsilon_v$ curve by $\dot{\varepsilon} = (\Delta\varepsilon_v/\Delta\varepsilon_a)\dot{\varepsilon}_a$. Then the radial strain rate $\dot{\varepsilon}_r = 1/2(\dot{\varepsilon}_v - \dot{\varepsilon}_a)$ and $\dot{\gamma} = 2(\varepsilon_a - \varepsilon_r)/\sqrt{3}$ are shown for the strain rate $\mu\varepsilon/s$ against the shear strain γ, where the compression strain is considered positive.

In the first stage of the loading, the shear strains γ are very small and the mobilized friction coefficient μ_m is not fully developed. However, under the extremely low effective stress conditions the viscous friction coefficient μ_v seems to have developed a peak, resulting in an increase in the total friction coefficient μ of the specimen. In

this stage, the abnormal high peak friction behavior is observed, as shown in Fig. 6. In the subsequent stage, the shear strain γ $\left(=2\sqrt{\varepsilon_{ij}\varepsilon_{ij}}=2\left(\varepsilon_{\mathrm{a}}-\varepsilon_{\mathrm{r}}\right)/\sqrt{3}\right)$ increases and the shear strain rate $\dot{\gamma}$ decreases due to a decreased volumetric strain rate as shown in Fig. 5. In this series of experiments, as the volume strain rate $\dot{\varepsilon}_{\mathrm{v}}=\dot{\varepsilon}_{\mathrm{a}}+2\dot{\varepsilon}_{\mathrm{r}}$ decreases and the axial strain rate $\dot{\varepsilon}_{\mathrm{a}}$ is kept a constant, the radial strain rate $\dot{\varepsilon}_{\mathrm{r}}$ decreases with γ increasing. The viscous friction coefficient μ_{v} decreases rapidly as the shear strain rate $\dot{\gamma}$ decreases according to Eqs. (2) and (5b). In the final stage for large strains when the mobilized friction coefficient μ_{m} moves against the limit of the critical friction coefficient μ_{s}, the volumetric strains are essentially constant. From Eq. (5), this results in a small viscous friction coefficient μ_{v} until it eventually diminishes. Thus, the total friction coefficient μ converges gradually towards the critical friction coefficient μ_{s} at this stage.

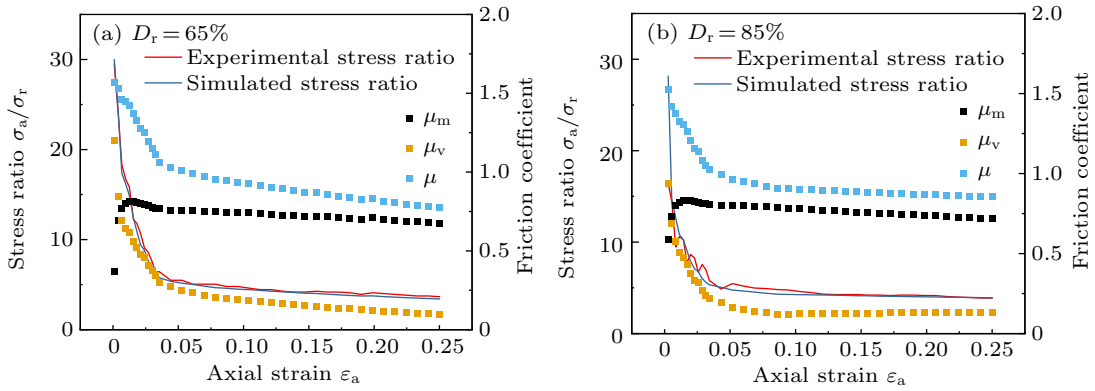


Fig. 6. Comparison between the unified model simulation results and the NASA microgravity tests on Ottawa sand ($\sigma_{\mathrm{r}}=0.05$ kPa) from the aspects of the principal stress ratio $\sigma_{\mathrm{a}}/\sigma_{\mathrm{r}}$ and the friction coefficient μ against the axial strains ε_{a}. The total friction coefficient μ is shown together with the viscous component μ_{v} and the quasi-static mobilized friction coefficient μ_{m}.

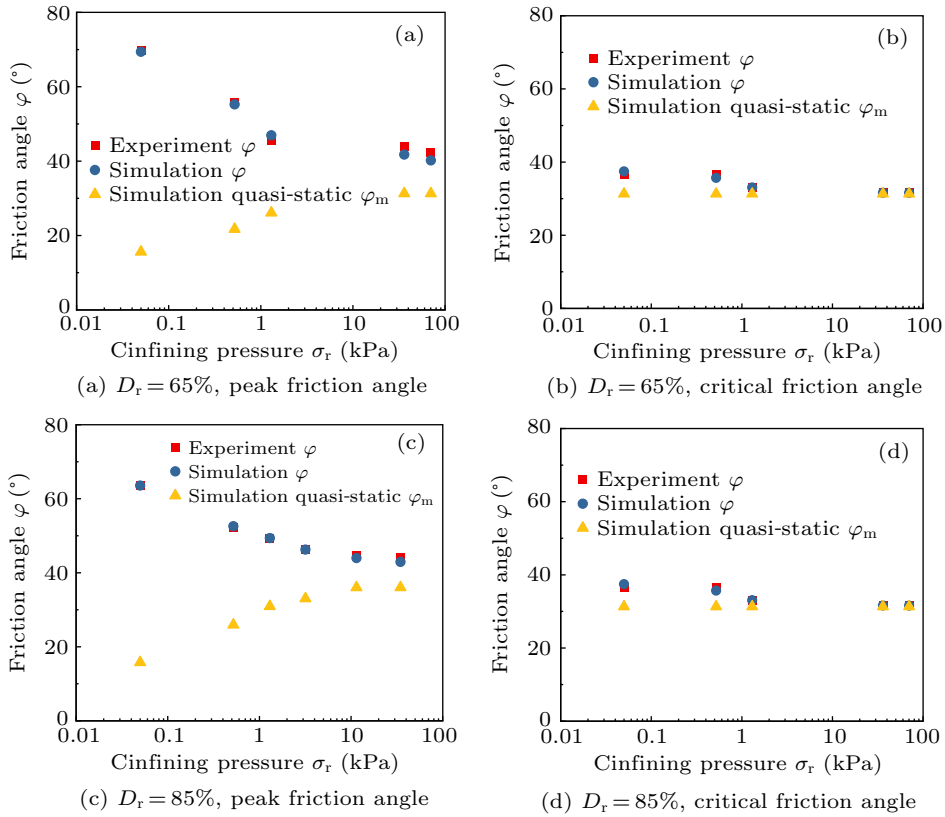


Fig. 7. Validation of the unified model using NASA microgravity tests data concerning the evolution of friction angle φ against radial stresses σ_{r}.

Based on the simulated friction coefficients μ_{m} and μ_{v} shown in Fig. 6, the peak φ_{p} and critical φ_{s} friction angles under the confining pressure of $\sigma_{\mathrm{r}}=0.05$ kPa were computed by substituting the peak and critical friction coefficients μ_{m} and μ_{v} shown in Fig. 7 into Eqs. (7) and (8). Similarly, all peak φ_{p} and critical φ_{s} friction angles under different confining pressures σ_{r} could be computed as well, as shown in Fig. 7 as a function of the radial stresses σ_{r}. Original experimental data

needed for these calculations have been listed in Table S1 from Section S1 of supporting information. The simulations show that the high peak friction angles φ_p occur for small radial or confining stresses σ_r. When the radial stresses σ_r increase, the peak friction angle φ_p decreases and converges towards the critical state friction angle φ_s. In this case, the peak friction angle of Ottawa sand increases rapidly with decreasing confining pressure below 1 kPa to 10 kPa, and remains essentially constant above that value of confining pressure. This pressure-sensitive behavior stems mainly from the constitutive characteristics of granular matter rheology, and in fact from a new physical insight shown in Fig. 3 — the inertial number is the determining factor, not just the strain rate. The specific confining pressure range, which of course varies depending on the granular material type and the type of shear experiment, can be influenced by the parameters listed in Table 1. One of the most influential fit parameters, I, we give the range of values of this parameter for general granular matter in Section S1 of supporting information.

The behavior shown in Figs. 6 and 7 concurs well with the results from the NASA microgravity tests and the conceptual framework of the unified model illustrated in Fig. 4. The high peak friction angle φ_p at much smaller shear strains γ observed in the NASA microgravity tests can be well explained by the "granular viscosity" for low effective stresses. For the investigated parameters, rapidly increased viscous friction coefficients occur at much smaller strain levels compared with conventional triaxial shear tests in a 1-g environment. This is the main reason for the abnormally high peak friction angles.

6. Conclusions

Triaxial tests performed by NASA–MGM on granular materials in a microgravity environment showed abnormally high peak friction angles for strain-rates that are commonly deemed quasi-static. Previous work by NASA–MGM have proposed a model based on rate-independent hyperelastic elastoplastic solid mechanics, and other researchers have investigated the microstructure of the material and possible sources of error to explain the high peak friction angles. However, neither the model proposed by NASA nor the detailed investigations into the microstructure and sources of error have been able to describe the phenomenon in a unified manner.

In this paper, we have proposed and demonstrated the ability of a unified model to accurately capture the behavior of the high peak friction angle. Our unified model includes rate-dependent and pressure-sensitive viscous effects within the framework of $\mu(I)$ rheology. The results have shown that the peak friction angle is dependent on the effective stress and strain-rate. For very low effective stresses or for high strain-rates, viscous effects become prominent and may become the main contributor to the high friction angles observed in the NASA–MGM microgravity tests. In these conditions, rate-independent models based on elastoplastic solid mechanics fall short.

In a microgravity environment, the effective stresses are very low. This creates a transient environment where viscous effects occur for strain-rates that are commonly deemed quasi-static in a 1-g environment. For small shear strains, the viscous effects are large due to the higher shear strain and volumetric strain-rates that are present. This results in the high peak friction angles. Towards the critical state, the shear strain-rate decreases due to the diminished volumetric strain rate for more moderate strains. This eventually results in an almost total elimination of the viscous effects for large strains. When the viscous effects are eliminated, the specimen enters the critical state where quasi-static effects dominate. In short, the viscous effects that result in the high peak friction angles are triggered by low effective stresses and increased shear strain rates (almost double the controlled axial strain rate in the NASA–MGM case). The unified model explains and mimics this behavior well, and the model agrees well with the results from the NASA–MGM microgravity tests under the selected material parameters. Further work should include investigations on the determination of the reference inertial number I_0 for various granular materials subjected to different conditions. Effects of narrow shear bands on friction angles of granular materials in low gravity conditions are yet to be investigated. Experimental investigations will have grand challenges on the measurements of non-uniform strains across the granular sample in low gravity conditions. In theory non-local rheological models are in need to develop.

Data availability statement

Some or all data, models, or code that support the findings of this study are available from the corresponding author upon reasonable request.

Acknowledgement

Project supported by the ESA-CMSA/CSU Space Science and Utilization Collaboration Program.

References

[1] Alshibli K A, Batiste S N and Sture S 2003 *J. Geotech. Geoenviron. Eng.* **129** 483
[2] Bagnold R A 1954 *Proc. Royal Soc. London A Math. Phys. Sci.* **225** 1160
[3] Atkinson J H 2007 *The mechanics of soils and foundations* (CRC Oress)
[4] Enomoto T, Koseki J, Tatsuoka F and Sato T 2015 *Soils Found.* **55** 1346
[5] Forterre Y and Pouliquen O 2008 *Annu. Rev. Fluid Mech.* **40** 1
[6] Jeremić B, Runesson K and Sture S 2001 *Int. J. Numer. Anal. Methods Geomech.* **8** 809
[7] Jiang Y and Liu M 2015 *Eur. Phys. J. E* **38** 15
[8] Jop P, Forterre Y and Pouliquen O 2006 *Nature* **441** 727

[9] Lee I K 1966 *J. Soil Mech. Found. Div.* **92** 79
[10] Li Z L, Tian Q and Hu H Y 2023 *Chin. Phys. B* **32** 034501
[11] MiDi G D R 2004 *Eur. Phys. J. E* **14** 341
[12] Sture S, Costes N C, Batiste S N, Lankton M R, AlShibli K A, Jeremic B, Swanson R A and Frank M 1998 *J. Aerosp. Eng.* **11** 67
[13] Tatsuoka F, Di Benedetto H, Enomoto T, Kawabe S and Kongkitkul W 2008 *Soils Found.* **48** 41
[14] Towhata I, Anh T T L, Yamada S, Motamed R and Kobayashi Y 2000 *Zero-gravity triaxial shear tests on mechanical properties of liquefied sand and performance assessment of mitigations against large ground deformation*, *Fifth International Conference on Recent Advances in Geotechnical Earthquake Engineering and Soil Dynamics*, 2010, San Diego, USA
[15] Wang Z H, Lü C, Xu Z W, Zhou E Q and Chen G X 2014 *Chin. J. Geotech. Eng.* **36** 1831
[16] Xiao S Z 2020 *Research on constitutive model and numerical simulation of sand rheology under low effective stress* Ph. D. Dissertation (Beijing: Tsinghua University) (in Chinese)